Geothermal Gradients in the Upper Amazon Basin derived from BHT data

Diego Barba[1], Roberto Barragán[2], Jonathan Gallardo[3], Andres Ormasa[3], Alfonso Salguero[4]

[1] PETROAMAZONAS EP, Quito, Ecuador.
[2] PETRONAS, Kuala Lumpur, Malaysia.
[3] Universidad Central Del Ecuador, Quito, Ecuador.
[4] TRIBOILGAS. Quito, Ecuador.

Email address
diego_barba@petroamazonas.gob.ec (D. Barba)
Corresponding author

Abstract

The Upper Amazon Basin (UAB), present foredeep of the sub Andean retro-foreland basin, comprises Putumayo area (southeastern part of Colombia), Oriente area (eastern Ecuador) and Marañón area (northeastern part of Peru). Bottom Hole Temperature (BHT) from a regional well log database (1076 wells and 2957 logs) were analyzed using data discriminated according to drilling operations (i.e., log acquisition operations, cementing, formation test, tools misreading values), topography and shallow subsurface weathering conditions (i.e., temperature data from wells with depths below 305 m. were avoided). A new normalized database has been setup (1021 wells and 1399 logs). Analysis of this data set has allowed better understanding of the regional distribution of the geothermal gradient variations within the study area. The results indicate a mean uncorrected geothermal gradient (UCGG) for the UAB of 20.4 °C/km. The UCGG is a first approach based on well data with sufficient information and is useful for comparison purposes with other basins where corrected data is limited. In addition, a new computer-generated contour Geothermal Gradient Map (GGM) has been created, using 56 locations (with BHT values at 3 or more different depths, and temperatures in the range 23.4 to 44.4 °C). Two locations are in Colombia, twenty eight in Ecuador and twenty six in Peru. This map is useful in analysis data of UCGG due to its wide distribution along the basin. Finally, correction based on Horner´s method was applied to these datasets (with 3 or more BHT values at the same depth; time since circulation - TSC incremental), obtaining a Corrected Geothermal Gradient (HCGG) of 22.9 °C/km (46 wells and 153 logs). We recommend the use of this gradient for comparative reference purposes.

1. Introduction

The earth's thermal energy is the driving force for volcanism and mantle convection, and thus for most of the associated geodynamic processes and plate tectonics, like uplifting and subsidence, diapirism and overthrusting. These processes leave thermal traces in the Earth's crust that can be studied and interpreted with the appropriate methods (Clauser, 1999).

The Marañón-Oriente-Putumayo Basins constitute one of the more prolific oil provinces in South America with cumulative production of more than 2880 MMBO and the estimated recoverable resources is 3023 MMBO (Higley, 2001). The hydrocarbon potential let renewed interest in this province. Given the link between temperature and the various physical and chemical processes leading to hydrocarbon generation, it is relevant to understand the present geothermal regime and past thermal history of these basins (e.g. Tissot and Welte, 1984).

Higley (2001) used the term Putumayo-Oriente-Marañón province in the report for the World Energy Project of the USGS. The term geologic province refers to a spatial entity with common geologic attributes. A province may include a single dominant structural element such as a basin or a fold thrust belt, or a number of contiguous related elements (Klett at al., 1997). The elements in the Putumayo-Oriente-Marañón province of Higley (2001) correspond to the Sub-Andean Zone (SAZ), the Upper Amazon Basin (UAB), the Iquitos Arc and the Pebas wetland. These main tectono-sedimentary units depict the revised concept of foreland basin geometry defined by Decelles and Giles (1996), corresponding to the wedge-top, fore-deep, the fore-bulge and back-bulge basin; respectively (Roddaz et al., 2005).

The main tectonic elements of the Putumayo-Oriente-Marañón province are well defined from the satellite gravimetric map (Bonvalot, et al., 2012). In this paper, we are considering the fore-deep as the main geodynamic element and the focus of our study. The name of Upper Amazon Basin (UAB) was proposed initially by Feininger (1975) and corresponds to the fore-deep, where the thickest depo-center (at present day) is located, near the Ecuador-Peru boundary (Figure 1). Other names have been assigned to this fore-land basin, such as MOP (Marañón-Oriente-Putumayo) by Marksteiner and Aleman (1997) or NAFB (North Amazonian foreland basin) by Roddaz et al. (2005).

In the northern part, La Macarena High is separating the UAB from Los Llanos Basin, while in the southern part, the Cushabatay High separates the UAB from Ucayali Basin. On the other hand, the Napo Uplift, Pastaza Depression, Cutucú Uplift, Santiago Basin and Huallaga Basin, are part of the present-day sub-Andean wedge-top and corresponds to its western limit. These uplifts, which produced the Andean foothills, are young structures formed during late Miocene times (Cambell, 1970; Baby et al., 2004). The Cushabatay High, Huallaga Basin and the southern part of Santiago Basin are not included in this study. The Caguán sub-Basin has been excluded due to lack of information.

The area of study covers approximately 315,000 Km, and it was defined considering two aspects: first, the iso-line of +20 mgals including Cretaceous rocks; second, the distribution of analyzed wells and available information included along the fore-deep, the wedge-top and back-bulge zones (Figure 1).

2. Regional Settings

Regionally, UAB includes two main domains both parallels to their corresponding Andean strikes. The southern part, wider and deeper, has a NE-NW strike, whereas the northern domain has a SW-NE strike. The limit between these domains is clearly defined by a major lineament or deflection that not only marks the changes along the Andean strike but also coincide with the location of the thickest part of the fore-deep depocenter along the northwestern part of the Maranon Basin (Situche area, Barragan et al., 2014) and the southern ending of the Iquitos Arch (Figures 1 and 2). Also, this variation along-strike, from NNW-SSE in northern Peru to N-S in Ecuador, is accompanied with a change in the wide of the Andean belt defining this major morphologic feature named the Huancabamba deflection (De Loczy, 1970; Gansser, 1973; Cambell, 1975). Based on paleo-magnetic studies, Feininger and Silberman (1982), Mourier et al., (1988); Mitouard et al. (1990) and Kissel et al. (1992), associates the origin of the Andean bending to the accretionary processes evident along the northwestern margin of the South America plate, suggesting that the geodynamic evolution of northern Peru is closer related to the processes observed in northern Andes than to those classically assumed for the Peruvian Andes. Finally, a second change along-strike is defined to the north, and is matching clearly with the pass from two Andean ranges in Ecuador to three ranges in Colombia, basically the Eastern cordillera of Colombia is absent in Ecuador. The Inter-Andean valley of Ecuador is not present in Colombia (e.g. Tibaldi et al., 2007). We had called to this knick-point as Chingual deflection (Figure 1) and believe that is a consequence of the oblique accretionary

processes of Caribbean plateau and associated volcanic arcs along the paleo margin (Mourier et al., 1988; Vallejo et al., 2009).
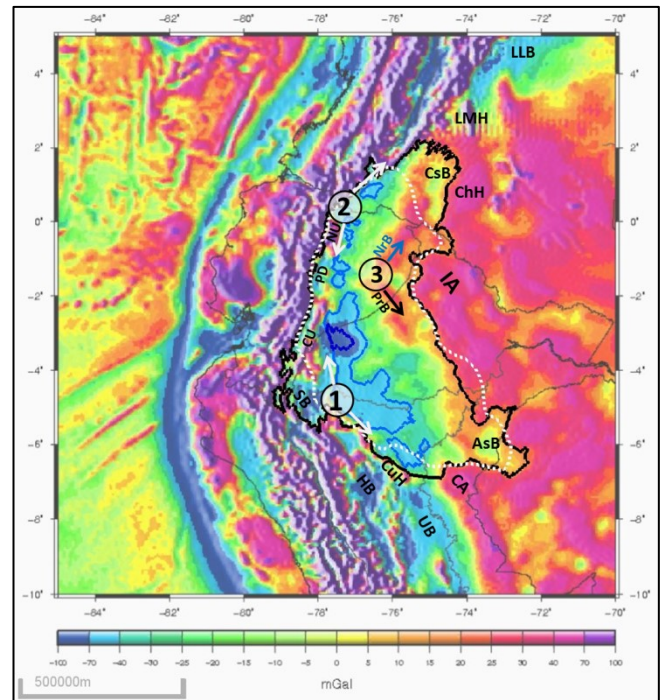

Figure 1 - The gravity anomaly map of Upper Amazon Basin (UAB.) It outlines the main fore-deep zone of the retro-arc foreland system. Background map provided by http://bgi.omp.obs-mip.fr/data-products/Gravity-Databases/Land-Gravity-data. Areas delimited by gravity anomalies are highlighted in black (+20mgal), light blue (-40mgal) and dark blue (-100mgal). These delineate respectively the study area, deep and deeper parts of the basin. In this figure the border of study area was smoothed and modified to consider wells with information. Thus, white dashed line refers to areas with information used to elaborate the geothermal gradient map. These include Huancabamba deflection (1), Chingual deflection (2), Pintoyacu arrow-head (3), Napo uplift (NU), Pastaza Depression (PD), Cutucú Uplift (CU), Caguán Sub-Basin (CsB), Acre sub-Basin (AsB), Iquitos Arch (IA), La Macarena High (LmH), Contaya Arch (CA), Chiribiquete High (ChH), Cushabatay High (CuH), Santiago Basin (SB), Huallaga Basin (HB), Los Llanos Basin (LlB): Ucayali Basin (UB), Napo River Block (NrB), Pastaza River Block (PrB).

In the northern domain, stand out the pointed ending of the Iquitos Arch. To this structural configuration we assigned the name "Pintoyacu arrow-head". The shortening between the Iquitos Arch and the Andes in this point produces the Pastaza Depression, a tectono-sedimentary unit of the wedge-top that is separating the Napo Uplift and Cutucú Uplift. The eastern Ecuadorian Andes appear as a fold-and-thrust belt adjacent to a continental fore-deep, represented by the Pastaza mega fan, debouching into the Amazonian lowland (Bés de Berc et al., 2005). The Pintoyacu arrowhead is formed by the south segment of Pastaza river block, and the north segment Napo river block (Figure 1). Initially, White et al. (1995) recognized two intra-basin highs called as Aguarico Arch and Conocaco Arch, respectively.

With the exception of the late deposits of Quaternary age, the depositional record of UAB is contiguous and constitutes a rather homogeneous regional system of sedimentary sequences (Pindell and Tabbutt, 1995; Ma et al., 2017), however, each country had proposed different geological

86

International Journal of Terrestrial Heat Flow and Applied Geothermics. VOL. 4, NO. 1 (2021); P. 85-94.

units related to the group of facies present in their jurisdictions. On the other hand, the identified structures inside the UAB are related to orogenic processes (Catuneanu, 2004; Roddaz et al., 2010), at least since the Late Cretaceous (Baby et al., 2004).
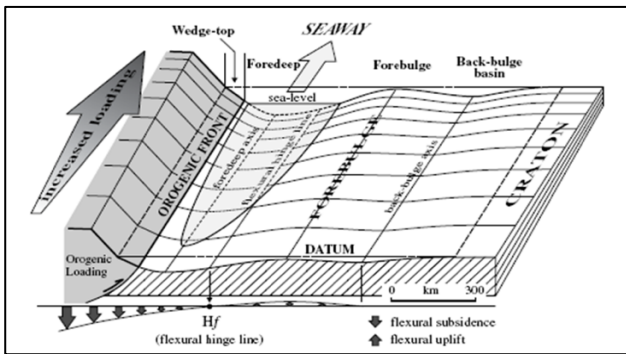

Figure 2 - Schematic depiction of the main elements of a retro-arc foreland system from Catuneanu (2004).

3. Data Analysis

In contrast to seismic, electric, magnetic and gravity surveys, geothermal studies are based primarily on data obtained from boreholes (Clauser, 1999). In order to constrain their relationship between main tectono-sedimentary units within the foreland basin and variations of the geothermal gradient, we compare the satellite gravimetric map (Figure 1) and regional geothermal gradient map elaborated with bottom hole temperature (BHT) data.

In the past, few efforts have been made in order to integrate and obtain functional representations (maps and profiles) at regional scale of the geothermal gradient along the UAB. In this regard, Alfaro et al. (2009) defined an average gradient of 29°C/Km for the Caguán-Putumayo basin, Colombia, based on BHT data corrected by the AAPG empirical method (Deming, 1989). Furthermore, a geothermal gradient map has been published by INGEOMINAS (2000) and by Alfaro et al. (2009) as part of INGEOMINAS-ANH project. In Ecuador, Hamza et al. (2005) calculated a geothermal gradient of 21.4°C/Km in the Oriente Basin based on well data from depth intervals of 1500–3500m. This work used corrected BHT by AAPG method using data compiled by Smith (1989). Also, Burgos et al., (2014) defined a gradient from uncorrected BHT of 22 °C/Km. Nevertheless, a geothermal isochrone map has never been prepared for the Ecuadorian Oriente Basin. In Peru, Henry and Pollack (1988) calculated a gradient of 24.5°C/km. Mathalone and Montoya (1995) proposed a gradient for the Marañón/Oriente basin as low as 20°C/km adjacent to the deformation front and increasing eastward up the foreland ramp to 35 – 40°C/km. Hamza et al. (2005) proposed a mean temperature gradient of 25.7 °C/Km for the Marañón basin using corrected BHT by AAPG method using data reported by Fuentes (1984) and Ocola (1985). Mathalone and Montoya (1995) show a coarse geothermal gradient map including the Marañón and Oriente areas but they did not specify either the used locations or the type of BHT information. Finally, Vela (2015) prepared a geothermal gradient map as part of the PERUPETRO-IRD project. In this case, the gradient was calculated from corrected BHT using Horner method, though no details are given.

Therefore, the scope of this work is to redefine the geothermal gradient along UAB and integrate this information with those from Putumayo, Oriente and Marañón areas. The gradient values were calculated by least square fits to temperature data from selected depth intervals. Also, geothermal gradient map was constrained using data of uncorrected BHT but considering values with a moderate to high confidence level. Additionally, we compared our result against those from earlier works correcting the BHT data according to AAPG method (Deming, 1989). Taking advantage of the significant data available, we propose an equation that relates the corrected geothermal gradient using the Horner method (HCGG) with uncorrected geothermal gradient (UCGG). The results obtained from this compilation can serve as inputs for future works about heat flow and to understand geodynamic processes.

Of importance for local and regional interpretations is the question of how well the data collected in boreholes characterize thermal field of the subsurface (Clauser, 1999). There are different ways to constrain the subsurface temperature data, depending of the accuracy. In order of importance these are: 1) high resolution temperature profiles; 2) Drill Stem Test (DST) and Repeat Formation Test (RFT); 3) Corrected Bottom Hole Temperature (BHT); 4) corrected Shallow Hole Temperatures (SHT); 5) geochemistry of spring water anomalies; 6) igneous and metamorphic petrology; 7) seismology; 8) uncorrected BHT; and 9) non-equilibrated temperature profiles (Sigismondi and Ramos, 2009). Additionally, pressure – volume – temperature (PVT) and build-up tests are additional methods to obtain more reliable temperature data.

High resolution temperature profiles and long-term static tests are also generally reliable, but they are rare and require a borehole with stable conditions. DST and RFT measurements are related to flow volumes of hydrocarbons or water from the producing formation and are generally the most reliable temperature data (Peters and Nelson, 2009). Data for PVT and build-up tests are available only for wells having potentially commercial reserves of hydrocarbons. BHT data are common but require correction because they are biased by a lower than true formation temperature. Nevertheless, uncorrected BHT can be used as a reasonable approach to estimate geothermal gradient. In the present work, these are used also for deriving the geothermal gradient maps.

On the other hand, the borehole temperature is an important parameter not only in the analysis of resistivity logs, but also in the detection of fluid movement. It is also employed in the analysis of fluid pressures, in geochemical modelling of formations and for assessment of maturity of hydrocarbons (Glover, 2014).

Prior to inserting the logging tool (e.g. wireline services), the borehole should be stabilized and cleaned, for which the drilling fluid is circulated in the well. The time employed in this operation is annotated in daily reports as circulation time (CT). After that, the ensemble of recording gets in the hole and go down until touch the bottom. The time measured refer to the interval when the pumps are turn-off and the arrival of the tool on the bottom. It is recorded as the time since circulation (TSC) in log-headers. Frequently, at least one run of logs is made in each section to assure a reliable Bottom Hole Temperature value.

87

International Journal of Terrestrial Heat Flow and Applied Geothermics. VOL. 4, NO. 1 (2021); P. 85-94.

During CT, the cold drilling fluid invades the formation and cools it down. Throughout TSC, the borehole gradually regains the true formation temperature, because of the large heat flux from the formation around the borehole. This heats the drilling fluid up to its ambient temperature, but the process is slow because it occurs via heat conduction which is less efficient than heat convection (Glover, 2014).

In the past years, it was common to calculate the geothermal gradient fixing a known value of temperature estimated at surface of the earth (e.g. Vaught, 1980), either from air temperature in the case of wells drilled onshore or water temperature in the case the wells drilled offshore. In fact, independent of the upper boundary condition, having a fixed surface temperature implies that the calculated gradient is biased and in many cases the gradient does not represent the true underground temperature profile registered (Barba, 2017). Currently, the method to define a gradient is by means of a linear regression, considering temperature data obtained at different depths (BHT in our case) and excluding data for shallow holes because of the strong influence of near-surface processes such as precipitation and movement of groundwater (Vaught, 1980; Hamza and Vieira, 2011).

A basic requisite for applying such corrections is the availability of multiple time-temperature data, after cessation of drilling activities. If multiple BHT measurements in the same depth are available, the Horner-plot correction procedure can be used (Deming, 1989). In the absence of this information, use of other empirical method is recommended, such as those suggested by the AAPG and described below.

Our study includes a data set of 2957 logs (L) carried out in 1076 wells (W). BHT data corresponding to depths above 305 meters was eliminated since these may be affected by environmental effects (Figure 3). Raw BHT data are, on average, cooler than true formation temperatures (Deming, 1989). However, they can give a primary proxy about the geothermal gradient of the basin.
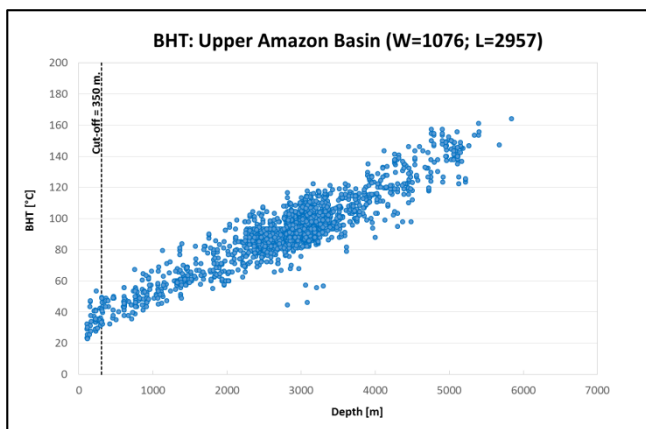

Figure 3 - BHT data available along the UAB. Data is not filtered and uncorrected. The letters W and L refer to number of wells and logs respectively.

3.1. General AAPG Correction

After filtering the original data set and eliminating spurious and shallow data, we get 1399 logs that correspond to 1021 wells. With this data set an UCGG was calculated (Figure 4a and 4b). Moreover, the filtered data is the basis for a proper Horner correction.

Among the empirical methods to correct the BHT, the most common is that stablished by the AAPG (e.g. Kehle et

al., 1970). The fit obtained between the equilibrium temperature and the observed BHT gave rise to a fourth order polynomial (Equation 1), where the temperature corrected is a function of depth (Z).

$$\Delta T = 1.9x10^{-3}Z + 8.5x10^{-7}Z^2 - 5.1x10^{-11}Z^3 - 1.7x10^{-14}Z^4 \qquad (1)$$

In the present work, we calculate the corrected BHT according to AAPG's method (ACGG) which allows easy comparisons with results of previous studies (Figure 4c).

The above procedure does not consider the effects of circulation time (CT) or time since circulation (TSC), information that in very few cases is preserved. However, the coefficients of this equation are unique to specific geographic areas (Vaught, 1980; Alfaro et al., 2009). Nevertheless, it has been widely used due to its ease of application. Examples are the coefficients of general equation derived from the average values defined in equations for data from West Texas and Louisiana areas (Deming et al., 1989; Sigismondi and Ramos, 2008; Alfaro et al., 2009).
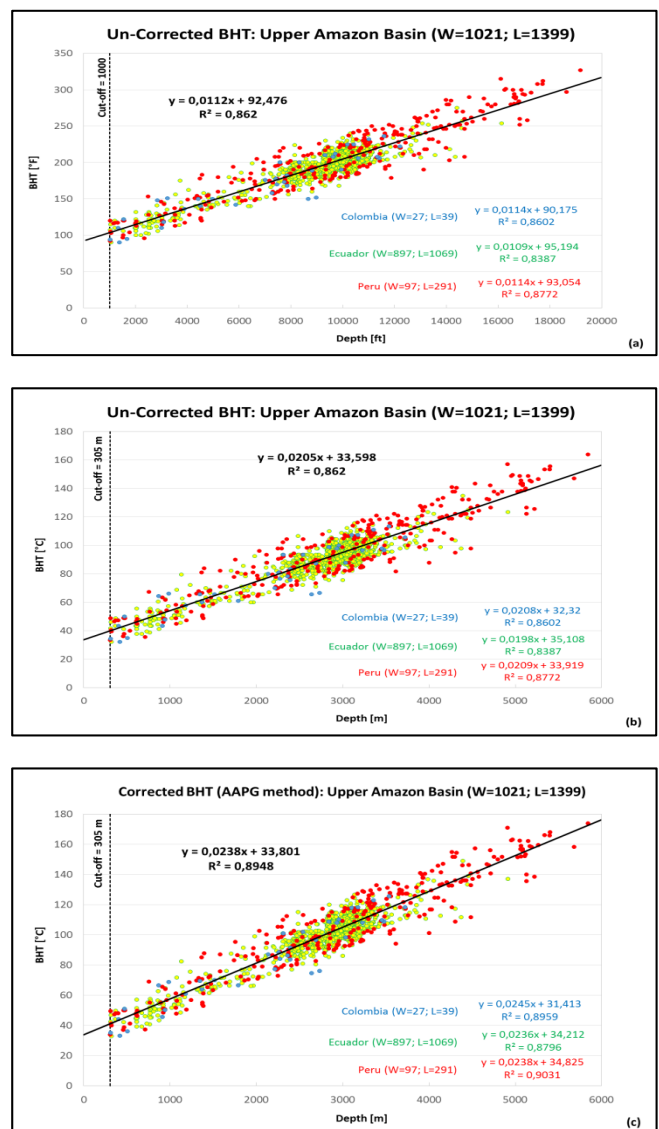

Figure 4 - Geothermal Gradient derived from uncorrected data (UC BHT) for UAB and each region political. (a) UCBHT plotted in Imperial Units, (b) UCBHT plotted in International System of Unit and (c) corrected BHT defined by AAPG method (Deming, 1989) and plotted in International System of Units.

88

International Journal of Terrestrial Heat Flow and Applied Geothermics. VOL. 4, NO. 1 (2021); P. 85-94.

Following this, a temperature versus depth correlation was built that incorporate trend-lines by linear regression method. Thus, the geothermal gradient is constrained, and a theoretical surface temperature defined. This process is repeated for each well, field, and basin.

In the "Putumayo basin", southeastern Colombia, the UCGG and ACGG were defined using 39 logs obtained from 27 wells. Its data series has a good depth distribution. The greatest depth reached come from the Unicornio-1 well with 3724 meters corresponding to a BHT of 106 °C. The uncorrected gradient defined is 20.8 °C/Km and the corrected gradient, calculated by AAPG method, is 24.5 °C/km.

For the Oriente basin of eastern Ecuador, the calculation was based on 1069 logs, derived from 897 wells. Its series of data show a very good distribution between shallow and medium depths, whereas at greater depths occur some data dispersion. Also, there is larger data accumulation between 2438 and 3353 meters (8000 and 11000 feet). This is related to the upper Cretaceous sections, which are the main reservoirs and productive interval in this part of the basin. The largest depth reached is 4916 meters in the Sacha Profundo-1 well, where the BHT is 123 °C. Finally, the UCGG calculated is 19.8 °C/Km and ACGG is 23.6 °C/km.

For the Marañón basin of northeastern Peru, an uncorrected gradient was calculated using 291 logs derived from 97 wells. In this case, five wells coming from the northern part of the Santiago Basin were included in this computation. The data series have a good distribution throughout the section. The greatest depth reached is 5843 meters in the Situche Central-3X well with a BHT of 164 °C. This well was drilled in the deepest part of the UAB depocenter. The UCGG defined is 20.9 °C/Km and ACGG is 23.8 °C/km.

In general, the gradients defined in Colombia and Peru are a bit higher than the one in Ecuador, similar observation to what was reported by previous authors (e.g. Hamza et al., 2005).

$$UCBHT = (0.021 * Depth) + 33.6 \qquad (2)$$

The gradient defined for the UAB, considering uncorrected BHT (UCBHT), is of 20.5 °C/Km assuming a theoretical surface temperature of 33.6 °C (Equation 2). The same was computed using a lineal regression through 1399 pairs of data from 1021 wells. This uncorrected gradient in the future can be compared with a corrected gradient and thereby find up if there is a correlation between them.

3.2. Correction for Fluid Circulation

Moreover, we calculated the corrected BHT using Horner's method (HCBHT) in order to constrain an accurate regional geothermal gradient.

The Horner correction was initially conceived by Bullard (1947) and later developed by Horner (1951). The CT is an important parameter in the Horner plot method and should therefore be determined accurately. Since injection of cold drilling fluid reaches different depths at different times, the circulation time varies with depth (Gíslason, 2014).

The BHT reported in each run increase with TSC. The Horner's correction search defines the equilibrium temperature, considering the relationship between CT and TSC. Thus, Horner correction is recommended if a set of three of more self-consistent BHT from a given depth are available. Temperature can be in Fahrenheit or Celsius and CT and TSC in hours.

$$Horner\text{-}time = (CT+TSC) / TSC. \qquad (3)$$

The accuracy of the Horner plot is limited by the simplifying assumptions made in its derivation, and by the lack of information on parameters such as duration of mud circulation (Deming, 1989). If there is no CT information available, a simple approach is using a time factor of 1 hour to obtain a minimum Horner correction. However, if there are several CT registered in a zone, it is better to calculate the trend-line and use CT value according to depth drilled (Figure 5).
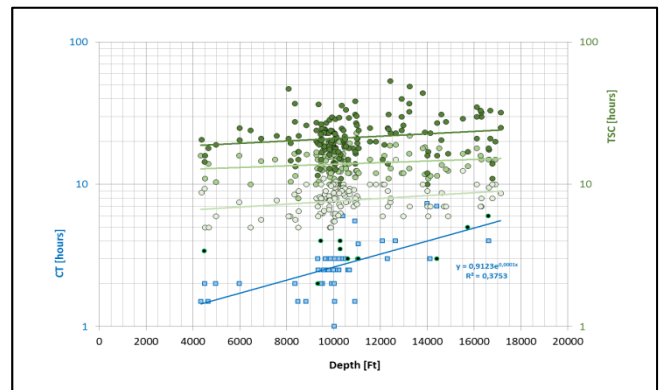

Figure 5 - Data along the UAB used to calculate the correction by Horner's method. CT from Final Drilling Report and TSC from log-header.

The corrected BHT represents the estimated formation temperature and is calculated by the Horner-plot method using the measured temperatures at a given depth from different logs, and the Horner-time. The temperature recovery data is plotted logarithmically with the Horner-time (Figure 6). The temperature will gather up as a straight line at infinite time. After an infinite time (Horner time of unity), the system is assumed to have stabilized and it is then possible to determinate the formation temperature. This is done by plotting the well temperatures as a function of Horner time and drawing a line of best fit (Gíslason, 2014).
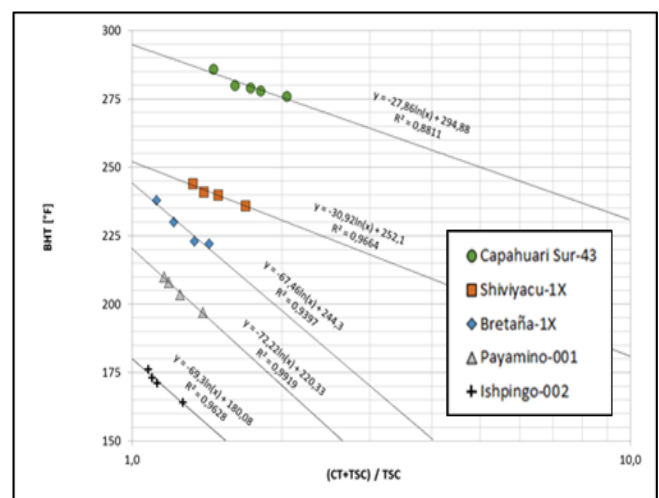

Figure 6. Horner plot used for formation temperature estimation along the UAB. The best fit line intersects Horne- time = 1 at the formation temperature. For comparison purposes five examples from wells along the basin are shown.

89

For the UAB, forty-six (46) wells with CT information were used in the Horner correction (Figure 5). In order to get an accurate geothermal gradient, each well should count with at least three measured of BHT at the same depth (Figure 6) and at less three BHT measured at different depths (Table 1). These conditions should be mandatory for wildcat wells. Moreover, in petroleum field with an unknown geothermal gradient, the coming development wells should consider a different logging plan with the aim to get more information and permit appropriate calculations.

The gradient defined for the UAB, considering HCBHT, is 23 °C/Km with a Theoretical Surface Temperature of 33.5 °C; it was computed using a lineal regression through 153 pairs of data with a good distribution throughout different depths and without dispersion.

$$HCBHT = (0.023 * Depth) + 33.5 \qquad (4)$$

The CGG shows a good correlation when is compared with PVT data. Unfortunately, this work only covers PVT data from ecuadorian's wells. However, the lack of PVT in greater depths is considered such as a bias; its trend-line is marked and can considerate as useful in order to compare with HCGG (Figure 7). Therefore, the HCGG can be applied in subsequent works and to compare with other basins around the world.
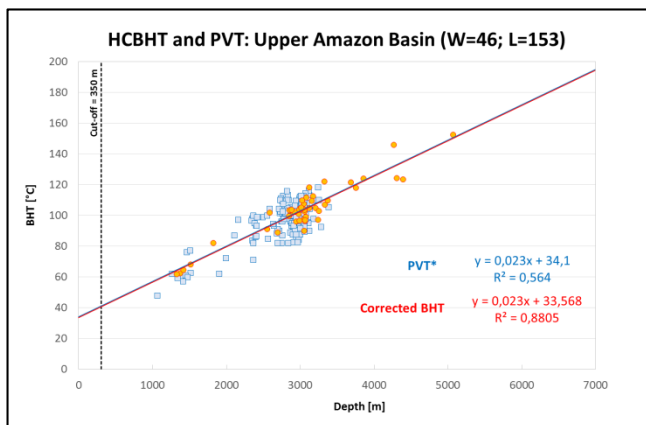

Figure 7 - Geothermal Gradient for UAB calculated since corrected BHT using the Honmer method. PVT coming only from Ecuador.

We proposed an equation of correlation between the HCGG and UCGG for the UAB. Considering that BHT is dependent of the depth, and that the correlation between them will be in the same depth, proceed to replace the Equation (2) in the Equation (4).

$$CBHT\_UAB = (1.12 * UCBHT) - 4.19 \qquad (5)$$

Thus, we can correct any BHT acquired in UAB, without being necessary to know the CT and TSC. However, it is recommended to follow all operational steps to achieve the information necessary to apply the Horner correction.

3.3. Geothermal Gradient Map of Upper Amazon Basin

Previous geothermal gradient maps were derived using BHT and applying a fixed surface temperature. Although, this technique has the positive benefit of incorporating plenty of data, it is possible that the resulting gradient does not provide representative values. Unfortunately, the data

available in the UAB allows calculation of its geothermal gradient using corrected BHT values by the Horner method but do not permit generation of geothermal gradient maps.

To avoid the use of non-representative gradients, we propose the use of filtered data by means of a quick confidence evaluation (QCE). Each confidence level corresponds to the product of the number of BHTs with a window of variation of the surface temperature, both normalized to unity (Table 1). The product obtained is classified in four categories, considering for our geothermal gradient mapping the trustworthy (>0.75) and Useful (>0.50) ones. In this way, our map considers well locations with at least three BHT (at different depths) and a theoretical surface temperature between 23 and 44°C (74 and 112 °F). Gradients with a confidence level between 0.26 and 0.50 were used as a reference to check the trend of the iso-lines generated by extrapolation. A summary of the parameters proposed is provided in Table 1.

Table 1 - Quick confidence evaluation (QCE) proposed for the Upper Amazon Basin (UAB). This analysis considers the number of BHTs available to different depths for each well and their corresponding calculated superficial temperature (Tsup).

	No. BHT			
1,00	>3	0,50	0,75	1,00
0,75	3	0,38	0,56	0,75
0,50	2	0,25	0,38	0,50
	max	121	112	102
	min	65	74	84
	Tsup = 93°F	±30%	±20%	±10%
		0,50	0,75	1,00

	Trustworthy
	Useful
	Only tendence
	Of no use

The data set used to create the uncorrected geothermal gradient map (UCGGM) of UAB are listed in Tables 2a, 2b and 2c.

The present-day geothermal gradient map of UAB considered data from wildcat wells, fields and occasionally clusters, the last term refers to grouping of nearly several wells but corresponding to different structures. The map shows a moderate gradient (22 and 27 °C/Km) along UAB.

The geothermal gradient is higher in the Bermejo and Yurimaguas areas found in Cutucú-Santiago and Huallaga basins (Figures 1 and 8). The high thermal regime observed in the Peruvian wedge-top, in the Yurimaguas zone, is related with Cretaceous rocks outcropping in the wedge-top and can be associated with the Huancabamba Deflection. The moderate to high thermal regime detected in the Ecuadorian wedge-top, near to the Bermejo area, is related with Cretaceous rocks outcropping in the wedge-top and can be associated with Chingual Deflection.

Table 2a - Data set used to create the uncorrected geothermal gradient map of UAB in the Putumayo area.
*Well; **Field; ***Cluster.

Well ID	Easting (degree)	Northing (degree)	UCGG (°C/Km)
Conejo***	-76.93	0.82	22.3
Rio Pescado***	-75.91	1.31	14.6

90

International Journal of Terrestrial Heat Flow and Applied Geothermics. VOL. 4, NO. 1 (2021); P. 85-94.

Table 2b - Data set used to create the uncorrected geothermal gradient map of UAB. in the Oriente area.
*Well; **Field; ***Cluster.*

Well ID	Easting (degree)	Northing (degree)	UCGG (°C/Km)
Betano***	-77.08	0.06	17.0
Blanca***	-76.17	0.33	24.3
Capiron***	-76.47	-0.68	21.1
Cowi*	-76.35	-0.93	16.8
Cristal**	-77.16	0.15	17.7
Culebra**	-76.89	-0.49	21.2
Diamante*	-77.18	0.17	21.7
Fanny**	-76.36	-0.18	17.9
Garza*	-76.77	-1.83	20.4
Guayusa*	-76.78	-1.62	23.5
Ishpingo***	-75.63	-0.99	21.2
Jivino**	-76.63	-0.41	21.9
Lago Agrio**	-76.86	0.11	22.4
Limoncocha**	-76.66	-0.37	21.2
Manati*	-76.67	-2.04	20.1
Masaramu*	-76.96	-1.75	18.1
Palo Azul**	-76.98	-0.16	21.5
Pañacocha**	-76.02	-0.33	17.7
Paraiso**	-77.04	-0.35	21.2
Payamino**	-77.04	-0.45	21.4
Rumiyacu**	-76.92	-0.95	22.6
Sacha**	-76.88	-0.33	22.1
Shiripuno***	-76.73	-0.73	17.3
Shushufindi**	-76.64	-0.17	19.5
Tigrillo*	-76.67	-1.94	21.0
VHR**	-76.29	0.29	24.5
Villano**	-77.47	-1.50	16.2
Yampuna*	-76.69	-0.92	20.1

Table 2c - Data set used to create the uncorrected geothermal gradient map of UAB in the Marañón area.
*Well; **Field; ***Cluster.*

Well ID	Easting (degree)	Northing (degree)	UCGG (°C/Km)
Boa Este***	-76.27	-2.51	25.5
Bretaña***	-74.33	-5.21	19.3
Chapuli*	-77.09	-3.55	23.2
Corrientes*	-75.06	-3.81	19.5
Cunico*	-75.23	-4.77	23.9
Forestal*	-76.23	-2.30	24.5
Guineayacu*	-76.01	-4.15	22.3
La Frontera*	-74.66	-6.32	23.0
Loreto*	-75.57	-5.92	19.9
Marañon Centro*	-75.21	-4.85	22.1
Marañon Este*	-74.04	-4.46	24.3
Pauyacu*	-76.05	-4.74	22.6
Santa Lucia*	-75.04	-6.40	13.0
Shanusi*	-76,07	-5.95	14.4
Situche***	-77.37	-3.02	21.7
Tamanco*	-74.33	-5.84	21.5
Tapiche*	-73.94	-5.89	19.7
Tucunare*	-76.32	-2.99	25.0
Ungumayo*	-76.37	-4.18	21.9
Yarina*	-73.77	-5.23	20.1
Yurimaguas*	-76.13	-5.84	29.0
Caterpiza*	-77.65	-4.00	17.2
Dominguiza*	-77.82	-4.40	15.7
Tanguintza*	-77.96	-4.73	18.4
Piuntza*	-77.80	-4.11	16.8
Putuime*	-77.93	-4.38	17.7

Limitations arising from low data density and uneven geographic distribution do not permit to define correctly the South extension of the Bermejo anomaly and the North extension of the Yurimaguas anomaly.
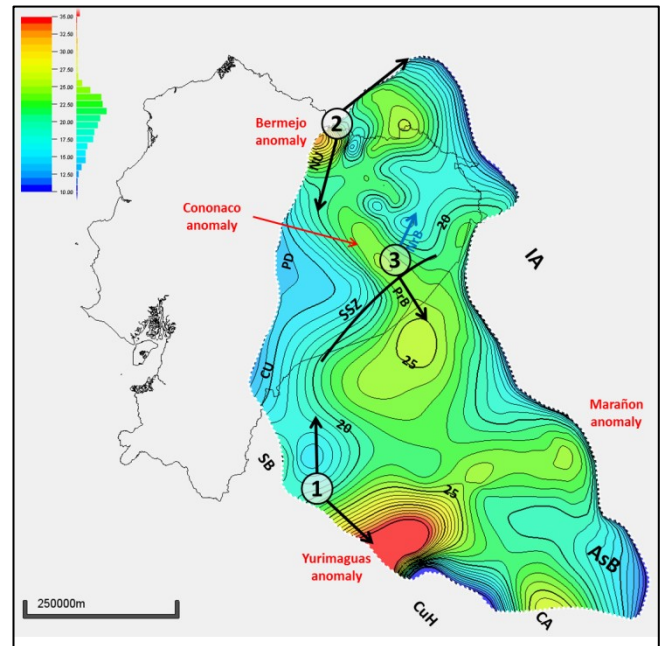

Figure 8 - Present-day Geothermal Gradient Map of UAB derived from Un-Corrected BHT data. It considers only certainty and useful Geothermal Gradient according to our Confidence evaluations. Contour Interval is 1 °C/Km. Huancabamba deflection No. 1. and Chingual deflection No. 2. Pintoyacu arrow-head No. 3. NU: Napo uplift; PD: Pastaza Depression; CU: Cutucú Uplift; CsB: Caguán Sub-Basin; AsB: Acre sub-Basin; IA: Iquitos Arch; CA: Contaya Arch; CuH: Cushabatay High; SB: Santiago Basin; HB: Huallaga Basin; LLB: Los Llanos Basin. NrB: Napo river Block; PrB: Pastaza river Block. SSZ: Shionayacu Shear Zone.

Lower gradients observed in the Corrientes and Acre (Solimoes) areas are separated by the high gradient identified as Marañón anomaly.

The low gradient observed in Acre sub-Basin will be related with the deeper and older Solimoes basin (Tankard, 2001). Wine et al. (2002) related low gradient values with areas of recent uplift, but more works about sub-surface mapping are necessary to confirm this idea.

Our integrated map of UAB has a good correlation with the map made in Colombia (c.f. Putumayo basin: ANH-INGEOMINAS Project: presented by Alfaro et al., 2009) and with the map made in Peru (c.f. Marañón basin: PARCEP Project, presented by Wine et al., 2002; and PERUPETRO-IRD project; presented by Vela, 2015). However, our map has a better distinction among high, medium and low gradients.

On the contrary, low gradients observed in the Cushabatay High, Santiago basin and Cutucú Uplift are associated with Paleozoic and Triassic-Jurassic rocks uplifted in the wedge-top zone. Wine et al. (2002) shows that the lowest gradients are seen along the Fold Thrusts Belt.

The geothermal gradient map shows two thermal regimes in the zone of Pintoyacu arrow-head, a higher gradient associated with Pastaza river Block (PrB) and a lower related with the Napo river block. The difference can be linked with the change of thickness of the sedimentary infill, being less in the Napo river Block (NrB). The Napo formation thins

91

northeastward and grades laterally into sandy facies indistinguishable from the underlying Hollín Formation (Campbell, 1970; Feininger, 1975; Canfield et al., 1982). Additionally, in the Napo river Block there are paleo-grabens infilled with Triassic-Jurassic rocks that have been uplifted by tectonically inversion. This petroleum play-fairway known as Capirón-Tiputini (Baby et al., 2004). Additionally, the Shionayacu Shear Zone (Tankard, 2001; Xie et al., 2010) displace the low gradient eastward of Cutucú Uplift-Pastaza Depression (Figure 8). The map of A-limestone marker prepared by Barba et al. (2017) shows the shear zone and agrees with Xie et al. (2010) about its dextral character. The details are given in Tables 2a (Putumayo area), Table 2b (Oriente area) and Table 2c (Marañón area).

4. Conclusions

A new Bottom Hole Temperature (BHT) database along the Upper Amazon Basin (UAB), the foredeep of the Andean retro-foreland basin, was obtained and normalized from a regional well log dataset (i.e., 1076 wells and 2957 logs). Analysis of this data set has allowed better understanding of the regional distribution of thermal gradients within the UAB study area at regional scale. The results achieved indicate an uncorrected geothermal gradient (UCGG) of 20.4 °C/Km assuming a surface temperature of 33.6 °C.

In addition, a Horner´s method correction was applied in this dataset obtaining a corrected geothermal gradient (CGG) of 23 °C/Km (from 46 wells and 153 logs). This gradient is in accordance to the PVT data coming from Ecuadorian UAB. The geothermal gradient value corrected by AAPG method (ACGG) was of 23.9 °C/km, a value similar to our results.

Two anomalies of moderate to high gradient are identified across the UAB, they were named as Marañón river (Peru) and Cononaco (Ecuador). These anomalies are more intense in the wedge-top zones, Yurimaguas and Bermejo areas, respectively. We suggest these anomalies could be related to change of the Andean strike and therefore, related to the Huacabamba deflection in the case of the Marañón river anomaly and to the Chingual deflection in the case of the Putumayo river anomaly.

Taking advantage of the significant data available, we will propose an equation that relates the corrected geothermal gradient by the Horner method (HCGG) with the uncorrected geothermal gradient (UCGG).

5. Acknowledgments

References

Alfaro C., Alvarado I., Quintero W., Vargas C., Briceño L. 2009. Mapa Preliminar de Gradientes Geotérmicos de Colombia, In: INGEOMINAS, ANH (Eds.), Proyecto Mapa Geotérmico de Colombia, p. 34.

Baby P., Rivadeneira M., Barragán R. 2004. Introducción. In: La *Cuenca* Oriente: Geología y Petróleo, 1ª edición. Travaux de l´Institut Francais d´Études Andines, 144, 13-20.

Barba, D. 2017. Gradiente Geotermal de las Cuencas de Ante-arco del Ecuador. Resúmenes extendidos de las VIII Jornadas en Ciencias de la Tierra, EPN, 5 p.

Barba D., Naranjo F., Chiriboga V., Cunduri J., Lamiña F., Jiménez L. 2017. Mapa Estructural del marcador Caliza A: Cuenca Oriente del Ecuador. VIII Jornadas en Ciencias de la Tierra; EPN – DG. Quito – Ecuador.

Barragán R., Chistophoul F., White H., Baby P., Rivadeneira M., Ramírez F., Rodas J. 2004. Estratigrafía Secuencial del Cretácico de la Cuenca Oriente del Ecuador. In: La *Cuenca* Oriente: Geología y Petróleo, 1ª edición. Travaux de l´Institut Francais d´Études Andines, 144, 55-102.

Bés de Berc S., Soula J., Baby P., Souris M., Chistophoul F., Rosero J. 2005. Geomorphic evidence of active deformation and uplift in a modern continental wedge-top fore-deep transition: Example of the eastern Ecuadorian Andes. Tectonophysics, 399, 351-380.

Bonvalot, S., Balmino, G., Briais, A.M., Kuhn, Peyrefitte, A., Vales, N., Biancale, R., Gabalda, G., Reinquin, F., Sarrailh, M. 2012. World Gravity Map. Commission for the Geological Map of the World. Eds. BGI-CGMW-CNES-IRD, Paris.

Bullard, E.C. 1947. The time necessary for a bore hole to attain temperature equilibrium. Geophysical Supplements to the Monthly Notices of the Royal Astronomical Society, 5(5), 127-130.

Burgos J., Baby P., Chistophoul F., Soula J.-C., Rocaht P. 2014. Cuantificación de las Erosiones Terciaria y Plio-Cuaternaria de la parte Sur de la cuenca Oriente, in: Baby P., Rivadeneira M., Barragán R. (Eds.), La Cuenca Oriente: Geología y Petróleo, Primera edición, Travaux de l'Institut Francais d'Êtudes Andines, tomo 144, 115-130.

Campbell C. 1970. Guide of Puerto Napo area, Eastern Ecuador with notes on the regional geology of the Oriente basin: Ecuador. Geol. Geophys. Soc., p. 40.

Campbell, C. 1975. Ecuador. In: World Regional Geology. Encyclopaedia of Earth Science. Springer, Berlin, Heidelberg. DOI https://doi.org/10.1007/3-540-31081-1_44.

Canfield R., Bonilla G., Robbins R. 1982. Sacha Oil Field of Ecuadorian Oriente. AAPG Bulletin, 66(8), 1076-1090.

Catuneanu O. 2004. Retroarc foreland system-evolution through time. Journal of African Earth Sciences, 38, 225-242.

Clauser C. 1999. Thermal Signatures of Heat Transfer Processes in the Earth's Crust. Springer (Eds.), Germany, p. 125.

Chistophoul F., Burgos J., Baby P., Soula J.-C., Bès de Berc S., Dávila C., Rivadeneira M. 2014. Dinámica de la

Cuenca de Ante-País Oriente desde el Paleógeno: Relaciones Tectónica-Erosión-Sedimentación. In: Baby P., Rivadeneira M., Barragán R. (Eds.), La Cuenca Oriente: Geología y Petróleo, Tercera edición, Travaux de l'Institut Francais d'Êtudes Andines, tomo 144, 105-131.

DeCelles P., Giles K. 1996. Foreland basin systems. Basin Research, 8, 105-123.

Deming D. 1989. Application of bottom-hole temperature corrections in geothermal studies. Geothermics, 18, 775-786.

De Loczy, L. 1970. Tectonismo Transversal na América do Sul e suas Relações Genéticas com as Zonas de Fratura das Cadeias Meio-Oceânicas. Anais da Academia Brasileira de Ciências, 42, 185-205.

Feininger, T. 1975. Origin of Petroleum in the Oriente of Ecuador. AAPG Bulletin, 59(7), 116-1175.

Feininger T., Silberman M. 1982. K-Ar geochronology of basement rocks on the northern flank of the Huancabamba Deflection, Ecuador: U.S. Geological Survey, open-File Report 82-206, p. 23.

Fuentes, R., 1984. Estudio de las temperaturas de la cuenca Marañon, Unpublished Report 300-629-84. Department of Technology, Division of Exploration and Exploitation, Petróleos del Perú.

Gansser, A. 1973. Facts and theories on the Andes. Journal of the Geological Society, 129, 93-131.

Gíslason, G., 2014. Interpretation of formation temperature and pressure of well in the Peistareykir geothermal field. Unpublished Thesis, University of Iceland, p. 50.

Glover, P. 2014. Temperatures logs. Petrophysics Course Notes, GLG-66565, University Laval, Canada. In: https://superpetrophysics.com/courses/ultimate-petrophysics-cheatsheets/lectures/439712.

Hamza, V.M., Silva F., Gomes A., Delgadilho Z. 2005. Numerical and functional representation of regional heat flow in South America. Physics of the Earth and Planetary Interior, 152, 223-256.

Hamza, V.M., Vieira F.P. 2011. Climate Changes of the Recent Past in the South American Continent: Inferences Based on Analysis of Borehole Temperature Profiles. In: Blanco J., Kheradmand H. (Eds.), Climate Change - Geophysical Foundations and Ecological Effects, InTech, 113-150.

Henry, S.G., Pollack, H.N. 1988. Terrestrial heat flow above the Andean subduction zone in Bolivia and Peru. J. Geophys. Res., 93, 15153–15162.

Higley, D. 2001. The Putumayo-Oriente-Marañon Province of Colombia, Ecuador, and Peru: Mesozoic-Cenozoic and Paleozoic Petroleum System. U.S. Geological Survey, Digital Data Series 063, p. 40.

Horner, D. 1951. Pressure buildup in wells. In: Proc. 3rd World Petroleum Congress, Section II, 503-521.

INGEOMINAS, 2000. Mapa geotérmico de Colômbia. Escala 1:1500.000. V.1.0.

Kehle, R., Schoeppel R., Deford, R. 1970. The AAPG Geothermal Survey of North America, Geothermics, Special Issue 2, U.N Symposium on the Development and Utilization of Geothermal Resources, Pisa 1970, Vol. 2, Part 1, 358-367.

Kissel, C., Laj, C., Surmont, J., Macedo, O., Mitouard, P. 1992. South American active margin: Andean

deflections and crustal thickening. Bull. Soc. Géol. France, 163(4), 371-380.

Klett, T., Ahlbrandt, T., Schmoker, J., Dolton G. 1997. Ranking of the world's oil and gas provinces by known petroleum volumes: U.S. Geological Survey, Open File Report 97-463, 1 CD-ROM.

Ma Z., Chen H., Xie Y., Zhang Z., Liu Y., Yang X., Zhou Y., Wang D. 2017. Division and resources evaluation of hydrocarbon plays in Putumayo-Oriente-Maranon Basin, South America. Petroleum Exploration and Development, 44(2), 247-256.

Marksteiner R., Aleman A. 1997. Petroleum Systems along the Fold belt Associated to the Marañon-Oriente-Putumayo (MOP) Foreland Basin. In: Memorias del VI Simposio Bolivariano Exploración Petrolera en las cuencas Subandinas, Tomo II, 63-74.

Mathalone, J.M.P., Montoya, R. 1995. Petroleum geology of the sub Andean basins of Peru. In: Tankard, A.J., Suarez S., R., Welsink, H.J. (Eds.), Petroleum Basins of South America, 62. AAPG Memoir, 423–444.

Mitouard P., Kissel, C., Laj, C. 1990. Post-Oligocene rotation in southern Ecuador and northern Peru and the formation of the Huancabamba deflection in the Andean Cordillera. Earth and Planetary Science Letters, 98, 329-339.

Mourier T., Laj C., Mégard F., Roperch P., Mitouard P., Medrano F. 1988. An accreted continental terrane in northwestern Peru. Earth and Planetary Science Letters, 88, 182-192.

Ocola, L. 1985. Heat flow in Northeastern Peru: Maranon Basin (in Spanish). Third South American Symposium COGEODATA. No., 20, Lima, Peru.

Peters, K., Nelson, P. 2009. Criteria to determine borehole formation temperatures for calibration of asin and Petroleum system models. Article #40463 adapted from poster presentation at AAPG Annual Convention and Exhibition.

Pindell, J.L., Tabbutt, K.D. 1995. Mesozoic-Cenozoic Andean paleogeography and regional controls on hydrocarbon systems. In: Tankard, A.J., Suarez S., R., Welsink, H.J. (Eds.), Petroleum Basins of South America, vol. 62. AAPG Memoir, 423-444.

Roddaz M., Hermoza W., Mora A., Baby P., Parra, M., Christophoul, F., Brusset, S., Espurt, N. 2010. Cenozoic sedimentary evolution of the Amazonian foreland basin system. In: Amazonia, Landscape and Species Evolution: A Look into the Past, 1st edition, Hoorn C. and Wesselingh F. (Eds), 61-88.

Sigismondi, M., Ramos, V. 2009. El flujo de calor en la cuenca Neuquina: Parte 1. Petrotecnia, 1, 64-81.

Smith, L.R., 1989. Regional variations in formation water salinity, Hollin and Napo formations (Cretaceous), Oriente basin, Ecuador. Am. Assoc. Petroleum Geol. Bull. 73, 757–776.

Tankard A. 2001. Tectonic Framework of Basin Evolution in Peru. Report for PARCEP, Perupetro S.A. and Canadian Petroleum Institute, p. 23.

Tibaldi A., Rovida A., Corazzato C. 2007. Late Quaternary kinematics, slip-rate and segmentation of a major Cordillera-parallel transcurrent fault: The Cayambe-Afiladores-Sibundoy system, NW South America. Journal of Structural Geology, 29, 4, 664-680.

93

International Journal of Terrestrial Heat Flow and Applied Geothermics. VOL. 4, NO. 1 (2021); P. 85-94.

Tissot B., Welte D. 1984. Petroleum Formation and Occurrence. Springer-Verlag (Eds.), p. 679.

Vallejo, C., Winkler, W., Spikings, R.A., Luzieux, L., Heller, F., and Bussy, F. 2009. Mode and timing of terrane accretion in the forearc of the Andes in Ecuador, in Kay, S.M., Ramos, V.A., and Dickinson, W.R., eds., Backbone of the Americas: Shallow Subduction, Plateau Uplift, and Ridge and Terrane Collision: Geological Society of America Memoir, 204, 204-209, DOI 10.1130/2009.1204(09).

Vaught T. 1980. Temperature gradients in a portion of Michigan: A review of the usefulness of data from the AAPG geothermal survey of North America. National Technical Information Service, U.S. Department of Commerce, p. 44.

Vela, Y. 2015. Modelado geoquímico 1D de las cuencas subandinas peruanas (Marañón, Santiago, Huallaga, Ucayali y Madre de Dios) y modelado 2D de las secciones balanceadas de las cuencas Marañón-Huallaga y Ucayali. Tesis Inédita, Universidad Mayor de San Marcos, p. 267.

White H., Skope R., Ramírez F., Rodas J., Bonilla G. 1995. Reservoir characterization of the Hollín and Napo Formations, Western Oriente Basin, Ecuador, In: Tankard A., Suarez R., Welsink H (Eds.), Petroleum Basins of South America. AAPG Memoir 62, 573-596.

Wine G., Arcuri J., Martínez E., Fernandez J., Calderón Y., Galdos C. 2002. Marañón Basin Technical Report, in: The Hydrocarbon Potential of NE Peru: Huallaga, Santiago and Marañón Basins Study, PARSEP (Eds.), 1, p. 625.

Xie J., Ji H., Su Y., Hu Y. 2010. Petroleum geology and exploration potential of Oriente-Marañón Basin. Petroleum Exploration and Development, 37(1), 51-56.

94

International Journal of Terrestrial Heat Flow and Applied Geothermics. VOL. 4, NO. 1 (2021); P. 85-94.